NEOPLASIA
www.neoplasia.com

Volume 23 Number 1 Month 2021 pp. 49–57 49

Spectroscopic investigation of radiation-induced reoxygenation in radiation-resistant tumors ☆, ☆☆

Sina Dadgar [a]; Joel Rodriguez Troncoso [a]; Eric R. Siegel [b]; Natalie M. Curry [a]; Robert J. Griffin [c]; Ruud P.M. Dings [c]; Narasimhan Rajaram [a,1,*]

[a] Department of Biomedical Engineering, University of Arkansas, Fayetteville, AR, USA
[b] Department of Biostatistics, University of Arkansas for Medical Sciences, Little Rock, AR, USA
[c] Department of Radiation Oncology, University of Arkansas for Medical Sciences, Little Rock, AR, USA

Abstract

Fractionated radiation therapy is believed to reoxygenate and subsequently radiosensitize surviving hypoxic cancer cells. Measuring tumor reoxygenation between radiation fractions could conceivably provide an early biomarker of treatment response. However, the relationship between tumor reoxygenation and local control is not well understood. We used noninvasive optical fiber-based diffuse reflectance spectroscopy to monitor radiation-induced changes in hemoglobin oxygen saturation (sO_2) in tumor xenografts grown from two head and neck squamous cell carcinoma cell lines – UM-SCC-22B and UM-SCC-47. Tumors were treated with 4 doses of 2 Gy over 2 consecutive weeks and diffuse reflectance spectra were acquired every day during the 2-week period. There was a statistically significant increase in sO_2 in the treatment-responsive UM-SCC-22B tumors immediately following radiation. This reoxygenation trend was due to an increase in oxygenated hemoglobin (HbO_2) and disappeared over the next 48 h as sO_2 returned to preradiation baseline values. Conversely, sO_2 in the relatively radiation-resistant UM-SCC-47 tumors increased after every dose of radiation and was driven by a significant decrease in deoxygenated hemoglobin (dHb). Immunohistochemical analysis revealed significantly elevated expression of hypoxia-inducible factor (HIF-1) in the UM-SCC-47 tumors prior to radiation and up to 48 h postradiation compared with the UM-SCC-22B tumors. Our observation of a decrease in dHb, a corresponding increase in sO_2, as well as greater HIF-1α expression only in UM-SCC-47 tumors strongly suggests that the reoxygenation within these tumors is due to a decrease in oxygen consumption in the cancer cells, which could potentially play a role in promoting radiation resistance.

Neoplasia (2021) 23, 49–57

Keywords: Oxygen consumption, optical imaging and spectroscopy, Radiation resistance, radiation therapy, Tumor oxygenation

Introduction

The majority of patients diagnosed with head and neck squamous cell carcinoma (HNSCC) present with locally advanced disease (Stage III or IV) [1] and are treated with a combination of surgery, radiation, and chemotherapy [2]. The treatment regimen can last several weeks and typically takes the form of daily radiation therapy—2 Gy/d; 5 d/wk for 7 wk – and weekly chemotherapy sessions. The delivery of radiation therapy in multiple fractions is hypothesized to cause cell death of oxygenated cells and leads to reoxygenation and radiosensitization of previously hypoxic cells [3–5]. Fractionated radiation therapy is believed to overcome the challenge of hypoxic tumors, which have been shown to be associated with poor long-term outcome [6–9]. Studies in patients and animal models using oxygen-sensing microelectrodes have offered evidence that an increase in tumor oxygenation or reoxygenation between dose fractions is associated with positive treatment response [10,11]. Despite providing absolute measures of oxygenation in tissue, these microelectrodes could disrupt the

* Corresponding author.
E-mail address: nrajaram@uark.edu (N. Rajaram).
☆ Funding: N. Rajaram acknowledges support from the Arkansas Biosciences Institute, the major research component of the Arkansas Tobacco Settlement Proceeds Act of 2000; the National Institutes of Health (R01CA238025, R15CA238861); and the National Science Foundation (1847347). R.P.M. Dings acknowledges funding from the Medical Research Endowment Fund, the Winthrop P. Rockefeller Cancer Institute, and the Center for Microbial Pathogenesis and Host Inflammatory Responses (P20GM103625).
☆☆ Conflict of interest: R.J. Griffin has ownership interest (including stocks, patents, etc) in IGF Oncology. The other authors disclose no potential conflicts of interest.
[1] Twitter: @RajaramLab
Received 11 September 2020; received in revised form 29 October 2020; accepted 3 November 2020

https://doi.org/10.1016/j.neo.2020.11.006

microenvironment when inserted into the tumor and are therefore not amenable to repeated measurements.

In contrast to microelectrodes, diffuse reflectance spectroscopy is an optical fiber-based technique that can noninvasively quantify hemoglobin oxygen saturation within a sampled tissue volume. Diffuse reflectance spectroscopy (DRS) is sensitive to light absorption by hemoglobin, the primary oxygen carrier in blood, and can determine the concentrations of oxygenated and deoxygenated hemoglobin present and hence allow calculation of hemoglobin oxygen saturation [12,13]. Measurements of hemoglobin oxygen saturation from tumors with DRS have been shown to be concordant with simultaneous pO_2 measurements using oxygen-sensing microelectrodes [14,15]. In addition, we have found a significant negative correlation between vascular oxygenation and immunohistochemical assessment of tumor hypoxic fraction [16]. Leveraging the noninvasive capabilities of DRS and its sensitivity to tumor hemoglobin oxygen saturation, Hu et al found that early reoxygenation during the treatment regimen was associated with treatment failure whereas late reoxygenation about 10 d after treatment was associated with local control in head and neck tumor xenografts [17]. These studies utilized a hypofractionated dosing schedule of 7.5 to 13.5 Gy/day for 5 consecutive days. Interestingly, previous work from our lab has also uncovered radiation-induced reoxygenation in radiation-resistant lung tumor xenografts in the first 24 to 48 h after radiation. These studies were conducted in a matched model of radiation resistance treated with conventional fractionation of 4 2 Gy doses over 2 consecutive weeks [18]. However, this work did not explore the mechanism of reoxygenation in the treatment-resistant tumors or relate reoxygenation to treatment outcome.

The primary goal of the current study was to determine radiation-induced changes in tumor oxygenation in head and neck tumor xenografts and investigate the association of this reoxygenation with tumor local control or recurrence. We used 2 previously characterized patient-derived HNSCC cell lines—UM-SCC-22B and UM-SCC-47 – to represent radiation sensitivity and resistance, respectively [19,20], and treated tumor xenografts with four 2 Gy fractions over 2 consecutive weeks (total dose of 8 Gy). We acquired optical spectra and quantified tumor oxygenation every day for 14 d, including immediately before and an hour after radiation on treatment days. Our results suggest that while reoxygenation patterns can be observed in both radiation-resistant and -sensitive tumors, the kinetics and source of this reoxygenation can be very different, depending on the radiation sensitivity. Given the importance of oxygen supply and consumption within a tumor and their roles in modulating response to radiation, these results shed light on the importance of longitudinal, real-time measurements of tumor oxygenation during radiation therapy to differentiate radiation responders from non-responders and hence improve response rates.

Materials and methods

Cell culture

Cell culture conditions have been reported previously [20]. Briefly, UM-SCC-22B (established from metastatic lymph node of a female patient, HPV-16 negative) and UM-SCC-47 (established from primary tumor of the lateral tongue of a male patient, HPV-16 positive) cells were purchased from EMD Millipore and were cultured in a mixture of Dulbecco's modified Eagle medium, 10% fetal bovine serum, 1% Penicillin–Streptomycin, 1% nonessential amino acids, and 1% L-glutamine. Oxygen consumption rate (OCR) of the cells were determined using a Seahorse metabolic flux assay as described previously [21]. Head and neck tumor xenografts were formed by injecting 1.5 million cells suspended in 1:1 mixture of Matrigel (Corning, New York) and saline into the right (treated group) or both (control group) flanks of nude mice (see tumor distribution in Supplementary Table 1).

Tumor xenografts and fractionated radiation treatment

All animal studies and protocols were approved by the Institutional Animal Care & Use Committee (IACUC) at University of Arkansas (Protocol number: 18,061). Athymic (nu/nu) mice were purchased from Jackson Laboratories and housed at the Central Laboratory Animal Facility (CLAF) of University of Arkansas under standard 12-h light/dark cycles with *ad libitum* access to food and clean water. Prior to cell injection, animals were allowed to acclimatize to animal facility conditions for 2 to 3 wk.

Animals in the treated (XT) groups underwent radiation treatment with four doses of 2 Gy over 2 consecutive weeks (8 Gy in total) [20] using an X-rad 320 biological cabinet (Precision X-Ray, North Branford, CT) (see treatment schedule in Figure 1A), while animals in the NT groups served as controls. Animals were placed in the center of a 20 × 20 cm X-ray radiation field. During radiation treatment, mice were kept under anesthesia using a mixture of isoflurane (1.5% v/v) and oxygen while the entire animal body was covered under lead blocks except the tumor. Greening et al have shown this combination and dose to closely mimic no anesthesia conditions [22]. Mice were monitored daily, and tumors were excised if (1) tumor volume reached 1500 mm^3(2) tumor necrosis was observed (3) other health related issues occurred. A subset of mice from each of the 4 groups was euthanized and tumors were excised at baseline, 24 and 48 h after a single 2 Gy dose of radiation (see Supplementary Table 2).

Diffuse reflectance spectroscopy

Our portable spectroscopic system consists of a tungsten halogen lamp (HL-2000, Ocean Optics, Dunedin, FL) as light source, a USB fiber optic spectrometer (Flame, Ocean Optics) for spectral light acquisition, and a bifurcated optical probe (dia.= 200 μm, NA = 0.22; FiberTech Optica, Kitchener, ON, Canada) for light delivery and collection. The probe tip was used for light delivery and collection and is equipped with four illumination and five detector fibers located at a source-detector separation distance (SDSD) of 2.25 mm with a sampling depth of approximately 1.8 mm [13]. We used a foot pedal controlled with custom LabVIEW software (National Instruments, Austin, Texas) for data acquisition. About 2–5 spectra in the wavelength range of 475 to 600 nm were collected and averaged optical properties were used to represent that tumor in temporal analysis. Because the surface area of our probe (32 mm^2) is always smaller than the surface area of typical tumor under investigation (average ~ 200 mm^2), we were able to collect multiple spectra from various parts of the tumor. Prior to any optical measurement from animals, reflected light intensity from an 80% reflectance standard (SRS-80–010; Labsphere, North Sutton, New Hampshire) was acquired to calibrate for daily variations in light throughput. Optical spectra from each tumor were recorded daily for a period of 14 d (see optical measurements schedule in Figure 1A) while animals were under anesthesia (1.5% v/v isoflurane mixed with 100% oxygen).

Extraction of optical properties

We employed an empirically generated lookup table (LUT)-based inverse model to fit the acquired spectral data and extract wavelength-dependent absorption and scattering properties of tumor [12]. To fit the model to acquired optical spectra, we made two assumptions as follows: (1) Light scattering has a negative power-law dependence on wavelength [23] as: $\mu_s'(\lambda) = \mu_s'(\lambda_0)(\lambda/\lambda_0)^{-B}$ with λ_0=600 nm as a reference point where light absorption is minimum. (2) Light absorption is the linear sum of light absorbing chromophores, namely oxygenated and deoxygenated hemoglobin, and animal skin. We calculated absorption coefficient as: $\mu_a(\lambda) = [Hb][\alpha\sigma_{HbO_2}(\lambda) + (1\text{-}\alpha)\sigma_{dHb}(\lambda)] + [MI]mel(\lambda)$, where [Hb] and [MI] respectively are total hemoglobin concentration and skin absorption. α is oxygen hemoglobin saturation representing the ratio of oxygenated

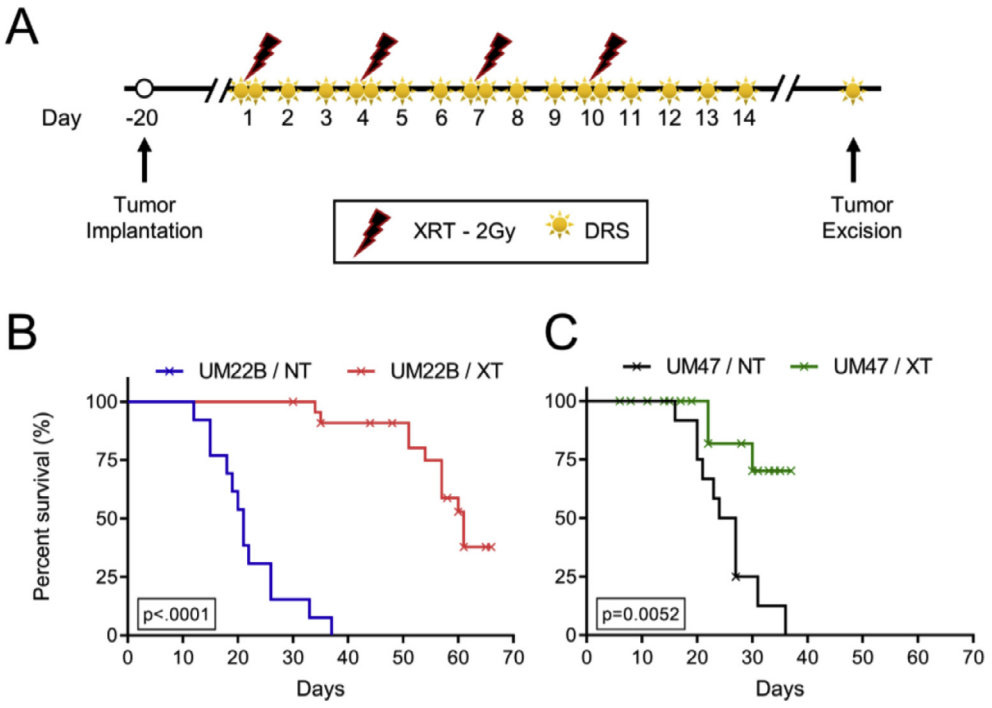

Figure 1. *S*tudy design for radiation-resistant and -sensitive tumors. **(A)** Timeline for the schedule of fractionated radiation and spectroscopic measurement. The lightning bolt signs indicate days of each fractions of radiation. Yellow sun signs indicate acquisition of optical spectra from the animals. On days of radiation, DRS spectra were collected immediately before and one hour after radiation. Comparison of the survival rate for control (NT) and irradiated (XT) animals bearing UM-SCC-22B **(B)** and UM-SCC-47 **(C)** tumors. *P* values based on log-rank test. Censored data points illustrated by x sign. (Color version of figure is available online).

(HbO_2) to total hemoglobin concentration [Hb]. The fixed absorption parameters related to extinction coefficients of hemoglobin and skin absorption were obtained from an online database [24]. We have previously reported the effects of pigment packaging to be minimal at wavelengths above 500 nm [25] and therefore did not include a correction factor to account for the effects of pigment packaging in light absorption. Data analysis was performed in MATLAB (MathWorks, Natick, MA).

Immunohistochemistry

An hour prior to euthanasia, mice were injected (i.p.) with Pimonidazole (60 mg/kg – Hypoxyprobe, Burlington, MA). After tumor resection and euthanasia, the flash-frozen tumors were sliced into sections of 10 μm using a cryostat (CM 1860; Lecia, Inc., Nussloch, Germany). We followed a direct labeling protocol in immunostaining of harvested samples [26]: After acclimatization to room temperature, slides were hydrated in PBS and a hydrophobic barrier was formed around each tissue section using a pap pen (Vector Laboratories, Burlingame, CA). Slides were fixed with 4% PFA, permeabilized using 0.5% Triton-X 100, and non-specific binding was blocked at room temperature using an in-house blocking solution (95% PBS + 4% goat serum + 1% sodium azide) for an hour. Slides were then stained with mouse monoclonal antibody conjugated to Dylight™ 549 fluorophore (Hypoxyprobe Red 549 kit; HPI, Inc, Burlington, MA). Serial slides were also incubated with primary HIF-1α rabbit antibody (NB100449 – NOVUS Biologicals, Littleton, CO) for 3 h at room temperature. The slides were next tagged with Alexa Fluor 488 goat anti-Rabbit (A-11,008, Thermo Fisher Scientific, Waltham, MA). The entire tumor section on each slide was imaged using a confocal microscope (Fluoview FV10i, Olympus) using a 10X objective (UPLSAPO10X, NA = 0.4, Olympus). Images acquired from individual regions of interest were stitched using the microscope software. Stitched images were binarized using a fixed threshold to separate pixels containing true signal from the background. This fixed threshold was identified from representative histograms where the signal of nonspecific background differed from the true signal. Four tumor sections were treated without Pimonidazole-specific and HIF-1α specific antibody to determine endogenous tissue autofluorescence, which was found to be negligible. Two tumor tissue sections were also incubated with secondary AF488 antibody without HIF-1α specific antibody to determine the presence of any nonspecific binding tissue section, which was found to be absent. Finally, percentage of Pimonidazole positive and HIF-1α positive pixels within each tissue section was calculated by dividing segmented pixels by the total number of tumor tissue pixels.

Statistical analysis

Survival analysis

Overall survival in each mouse was measured as the length of time in days from when the mouse's tumor reached 200 mm^3 to when the mouse was euthanized for excessive tumor size (defined as a tumor volume of $\geq$1500 mm^3). Since the animals from control groups were inoculated with tumors on both flanks, overall survival in a control-group mouse was marked as starting on the day when its first tumor reached the volume of 200 mm^3. Any animal that died for a reason other than excessive tumor size had its overall survival right-censored on the day of its death. The differences in overall survival between groups were compared statistically using the 2-sided log-rank test with $P < 0.05$ significance level, while the survival benefit with radiation therapy was quantified as the inverse of the Cox-regression hazard ratio comparing treated to control animals.

Analysis of tumor volume

Prior to statistical analysis, the raw volume data were logarithmically transformed with the aim of minimizing the correlation of group means with group standard errors. The transformed data then were analyzed

using repeated-measures analysis of variance (ANOVA) using the MIXED procedure in SAS v9.4 (The SAS Institute, Cary, NC). The analysis model for log-volumes employed an ante-dependence structure to model the covariance over time among the longitudinally collected data and utilized the Kenward-Roger method to determine test-statistic degrees of freedom. Within each cell line, the right flanks from control-group mice were compared to the right flanks from XT-group mice. Within each combination of cell line and treatment, mean log-volumes on subsequent days of growth were compared to their day 1 value. All comparisons employed an unadjusted $P < 0.05$ significance level (2-sided) despite the multiple comparisons, in order not to inflate Type II (false-negative) error.

Analysis of optical properties

Raw optical properties from day 1 through 14 from right flanks were normalized by treatment group to the group mean of the value it had on day 1. This way, values on day 1 have mean of 1 but individual values different from 1 (i.e., they show variability), and thus can be included in the analysis. The normalized data were then subjected as before to repeated-measures ANOVA using the MIXED procedure in SAS v9.4 software (The SAS Institute, Cary, NC). For each normalized optical property, the analysis model employed an unstructured autocovariance matrix to model the covariance between different measurements performed on the same tumor over time and utilized the Kenward-Roger method to determine test-statistic degrees of freedom. All comparisons between treatment groups or time points were conducted as previously described and employed an unadjusted $P < 0.05$ significance level (2-sided) despite the multiple comparisons, in order not to inflate Type II error.

Analysis of immunohistochemical data

We used the Wilcoxon rank sum test for statistical analysis of immunohistochemical data. All tests employed a 2-sided $P < 0.05$ significance level.

Results

Fig. 1B-C present the Kaplan-Meier curves for the UM-SCC-22B and UM-SCC-47 tumors, respectively. Animals growing UM-SCC-22B tumors that were irradiated (XT) survived significantly longer compared with nonirradiated controls (NT), with a mean survival of 56.4 vs. 21.9 d (log-rank $P < 0.0001$); the associated survival benefit with radiation treatment was 44.7 (indicating 44.7-fold higher survival for XT tumors) with a 95% confidence interval [CI] of 9.34–214. Although the heavy censoring in XT UM-SCC-47 tumors (Figure 1C) prevented us from seeing appreciable delay in mean survival compared with NT (mean survivals of 28.5 vs. 25.5 d), we still observed a significant difference in survival of the NT and XT groups (log-rank $P = 0.0052$) with an associated survival benefit of 5.51 (95% CI: 1.48–20.5) for XT groups.

Figure 2 presents measurements of tumor volume, hemoglobin oxygen saturation, and total hemoglobin concentration during and after radiation therapy of the UM-SCC-22B (left panel) and UM-SCC-47 (right panel) tumors. As early as day 2, fractionated radiation therapy resulted in significant differences between the volume of NT and XT groups of UM-SCC-22B tumors ($P< 0.0001$; illustrated in Figure 2A by black asterisk for day 2 and black forward arrow for following days). In contrast, there were no significant differences between the UM-SCC-47-NT and -XT groups, and mean tumor volumes in both groups were nearly identical for the first 7 days (Figure 2B). Importantly, tumor volumes in the UM-SCC-22B-XT group were significantly higher than baseline only after day 21 ($P = 0.001$); for all other groups, the increase in tumor volume was significant beginning day 2.

To determine radiation-induced changes in tumor oxygenation, we quantified the optical properties from the measured DRS spectra (Supplementary Figure SF1) and computed the fold-change in the measured parameters over time with respect to their preradiation baseline measures. Figure 2C-F illustrates the fold-change in hemoglobin oxygen saturation (sO_2) and total hemoglobin concentration (cHb). Radiation therapy did not cause significant changes in sO_2 or cHb in the UM-SCC-22B tumors (Figure 2C and E). There was a significant increase in sO_2 in the XT UM-SCC-47 tumors compared with pre-radiation baseline sO_2 ($P < 0.05$) and this significant reoxygenation trend was evident on several days over the 14-day period when these tumors were monitored (Figure 2D). The XT UM-SCC-47 tumors also showed a significant decrease in cHb compared with pre-radiation baseline (days 6, 7, 10, 13 and 14) and the NT group (days 6, 8, and 14) ($P < 0.05$; Figure 2F). Analysis of oxygenated (HbO_2) and deoxygenated hemoglobin (dHb) concentrations showed that the temporal decay in cHb and the increase in sO_2 in the UM-SCC-47 tumors could be attributed almost entirely to a decrease in dHb while there was no significant change in HbO_2 (Supplementary Figure SF2).

While there was an overall increase in tumor oxygenation in the UM-SCC-47 tumors over the 14-d period, we found that reoxygenation trend was cyclical, consisting of several rapid increases followed by decreases in tumor oxygenation. To investigate this cyclical nature of reoxygenation, we studied the short-term effects of radiation therapy on tumor sO_2 over the 48 h following each dose of radiation. Figure 3 presents data from 1, 24, and 48 h post-therapy for each of the 4 doses. In response to each dose of radiation, there was an increase in sO_2 in the UM-SCC-22B and UM-SCC-47 tumors 1 hour after radiation; this reoxygenation was statistically significant after the first, third, and fourth doses in the UM-SCC-22B ($P< 0.01$). After each dose, this increase in sO_2 was followed by a decrease to baseline levels over the next 48 h. Similarly, UM-SCC-47 tumors displayed an increase in mean sO_2 immediately after radiation that was followed by a large decrease at the 24-hour time point. However, at the 48-h time point, the mean sO_2 was greater than the preradiation baseline for that dose (Figure 3B). Within these cell lines, the radiation-induced changes in sO_2 appear to be driven by different factors in the UM-SCC-22B and the UM-SCC-47 tumors. The large increase in sO_2 in the UM-SCC-22B tumors immediately after radiation is due to a statistically significant increase in HbO_2. On the other hand, the increase in sO_2 in the UM-SCC-47 tumors is due to a decrease in dHb over time (Supplementary Figure SF3).

Reoxygenation following radiation has been shown to upregulate HIF-1α in tumors [27. Therefore, we examined the extent of tumor hypoxia and HIF-1α expression in the UM-SCC-22B and UM-SCC-47 tumors over the first 48 h following radiation therapy (Supplementary Table 2, Figure 4A, and Supplementary Figure SF4). Figure 4B-D presents the results of immunohistochemical assessment from tumor sections collected at baseline, 24 and 48 h after a single 2 Gy dose of radiation in the NT and XT groups. Our results indicate that in comparison to UM-SCC-22B tumors, UM-SCC-47 tumors have slightly higher hypoxic fraction and a significantly higher HIF-1α expression at baseline ($P = 0.02$). Radiation therapy had different effects on the hypoxic fraction and HIF-1 expression in the 2 tumor groups. We observed an increase in hypoxic fraction in the UM-SCC-22B tumors 24- and 48-h ($P= 0.03$) following radiation therapy and a trend toward decreasing hypoxic fraction in the UM-SCC-47 tumors. While we found no changes in HIF-1α expression in the UM-SCC-22B tumors following radiation, there was a trend towards a decrease in HIF-1α expression in the UM-SCC-47 tumors at the 48-h time point.

Discussion

Reoxygenation following radiation therapy has long been postulated to be an important mechanism in the radiosensitization of previously hypoxic cells within a tumor and has been shown to be an indicator of tumor response to radiotherapy. However, there is also evidence that reoxygenation following radiation is a double-edged sword because it can lead to radiation resistance. Temporal investigations of tumor reoxygenation are challenging because the

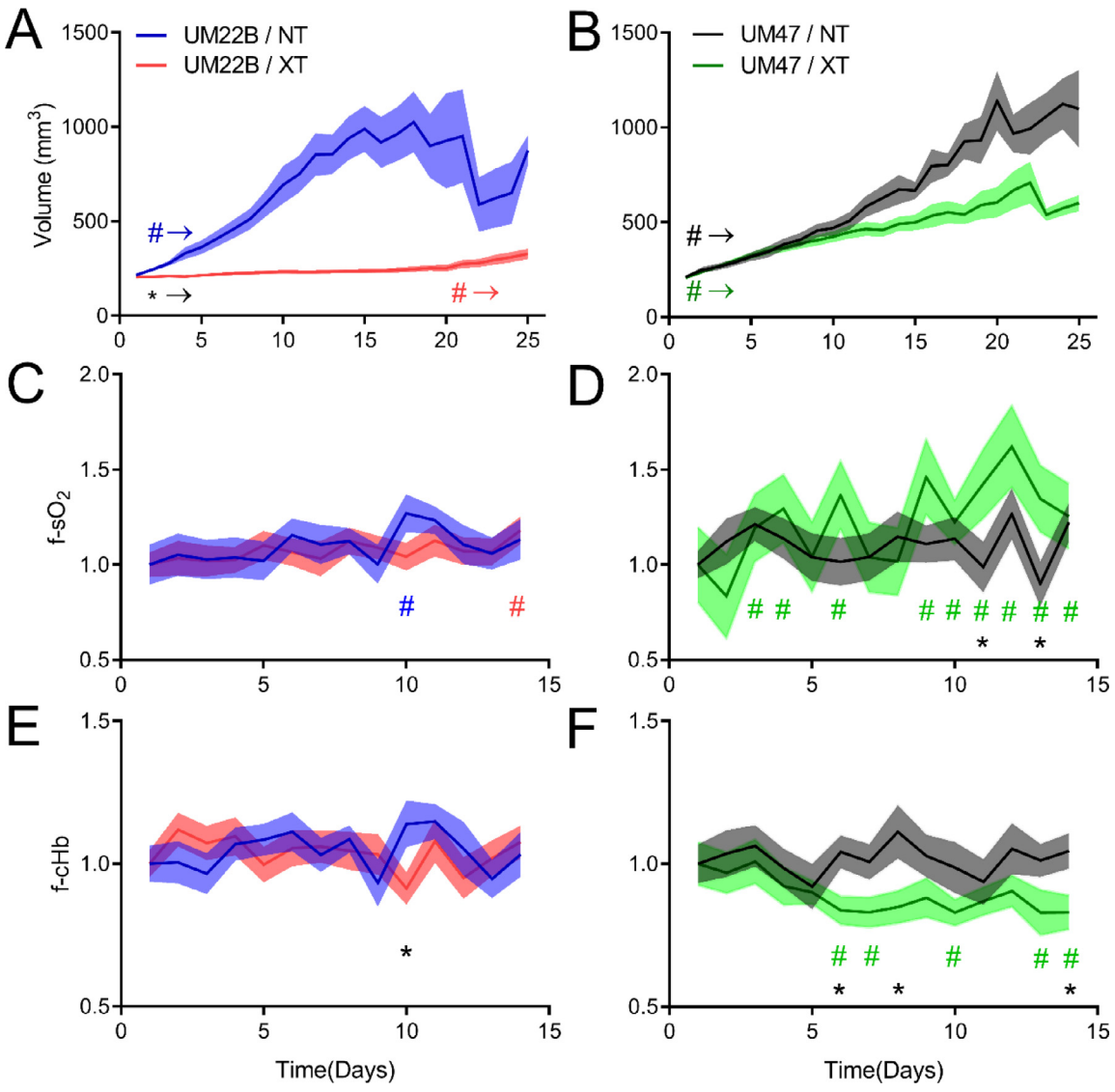

Figure 2. Tumor growth kinetics **(A and B)** are observed to identify radiation response of NT and XT groups among UM-SCC-22B and UM-SCC-47 tumors. Percent change in hemoglobin oxygen saturation sO_2 **(C and D)** and total hemoglobin concentration cHb **(E and F)** are observed over time to identify biomarkers of radiation-resistance. Data are presented as group mean (line) ± SEM (semitransparent shadow). Significant differences among NT and XT treatments in specific days are illustrated with black asterisks (*) while significant differences of specific days with respect to their own value in day 1 are illustrated using pounds (#). Arrows adjacent to the significance signs are indication of presence of significance until the end of study. * and # indicate statistical significance at $P < 0.05$. (Color version of figure is available online).

technologies utilized are either invasive (oxygen-sensing microelectrodes or tissue removal) or expensive (magnetic resonance imaging, positron emission tomography), and are not amenable to repeated measurements. DRS has been used in animal studies to identify differences between partial and complete responders based on differences in sO_2 in response to high doses of radiation/fraction (7–39 Gy) [17,28]. Our long-term clinical goal is to investigate whether using DRS to measure tumor functional changes in HNSCC patients, who are typically treated with dose fractions of 2 Gy, can be validated as a predictor of treatment response. Here, we used DRS to monitor the reoxygenation kinetics of HNSCC tumors with known radiation sensitivity.

Previous work has shown that the UM-SCC-22B tumors are sensitive to radiation therapy while the UM-SCC-47 tumors do not respond to therapy when treated with four doses of 2 Gy over 2 consecutive weeks [20]. While the outcomes for both cell lines in our study were largely consistent with this report, there was a significant difference in tumor growth delay in the UM-SCC-22B beginning the day after treatment, while the report by Stein et al found significant differences only beginning day 15. In fact, the mean tumor volume in the XT tumors remained unchanged during and up to 1 wk after 4 2 Gy fractions were administered over 2 wk. This corresponded to no significant change in tumor hemoglobin oxygen saturation over the 14 d of treatment monitoring, indicating that therapy had likely arrested cell proliferation within these tumors. It is important to note that while there were no long-term changes in sO_2 or cHb in the UM-SCC-22B tumors, there were immediate radiation-induced increases in oxygenation 1-h post-treatment (Figure 3) that are largely consistent with previous studies that utilize DRS to monitor radiation response [18,28]. Moreover, the control UM-SCC-22B and UM-SCC-47 tumor that grow at the same rate as the XT UM-SCC-47 tumors also show nearly no change in oxygenation with respect to baseline. A lack of reoxygenation has been

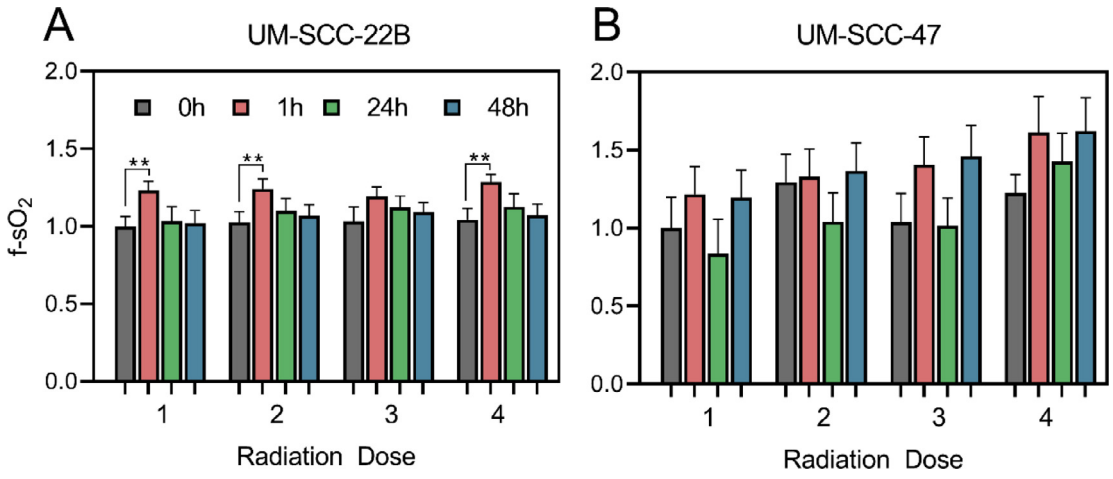

Figure 3. Temporal changes in optical properties in response to 4 doses of radiation. Changes in sO_2 **(A, B)** in response to 4 doses of radiation are illustrated at 4 time points: before (gray), 1 h (red), 24 h (green), and 48 h (blue) after radiation. Data are presented as group mean + SEM. ** indicates $P < 0.01$. (Color version of figure is available online).

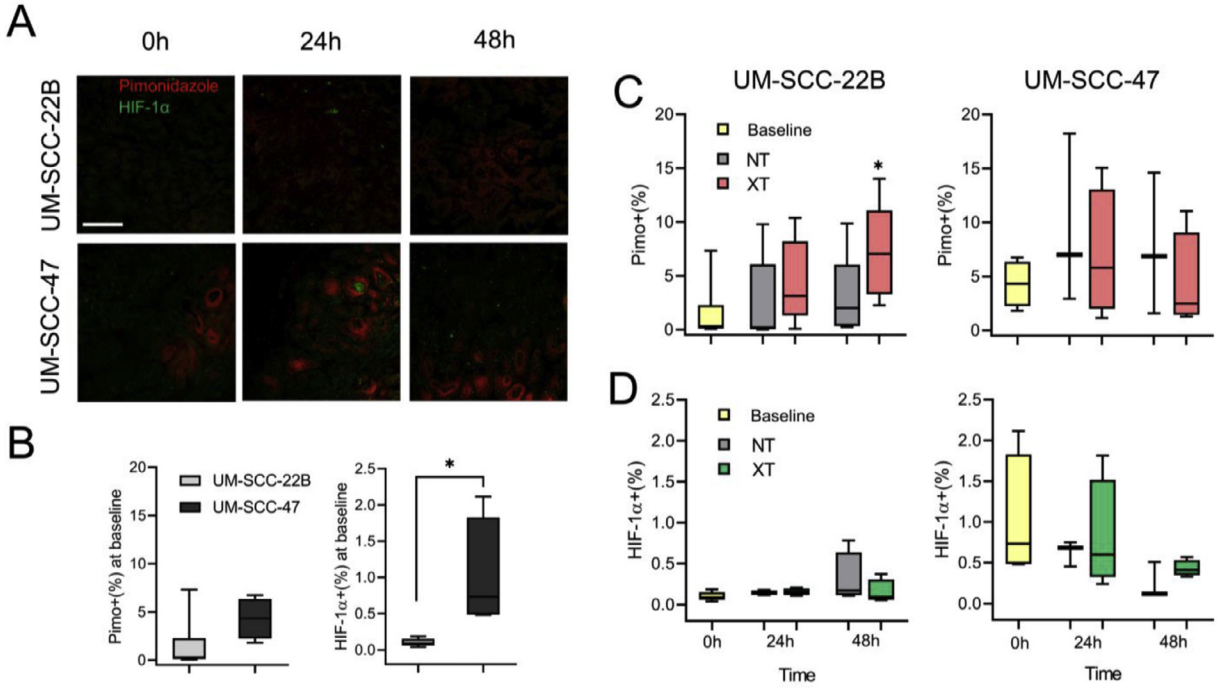

Figure 4. Immunohistochemical assessment of tumor hypoxia and HIF-1α in tumor tissue sections. **(A)** Representative images from UM-SCC-22B and UM-SCC-47 tumors excised at baseline, 24 and 48 h after radiation. The false-colored red and green signals respectively represent Pimonidazole positive and HIF-1α positive pixels. The scale bar represents 250 µm. Quantification of percentage of Pimonidazole positive and HIF-1α positive pixels in UM-SCC-22B and UM-SCC-47 tumors at baseline **(B)** and following time points **(C and D)**. (Color version of figure is available online).

observed in head and neck cancer patients about two weeks into daily treatment with fractionated radiation therapy (2 Gy/day) [8]. Stadler et al reported a statistically significant reduction in pO_2 and increase in hypoxic fraction in locally advanced HNSCC patients who were evaluated 3 wk after commencing fractionated therapy at 2 Gy/day. This decrease in pO_2 was observed in both complete and partial responders [29]. They attributed the observed reduction in pO_2 to reduction of blood flow in response to radiation. Conversely, increases in tumor oxygenation have also been reported in response to 5 doses of 2 Gy in head and neck tumor xenografts although the observed changes did not correlate with response/failure [11].

In contrast to the UM-SCC-22B tumors, we noted a significant increase in sO_2 in the UM-SCC-47 tumors which are relatively non-responsive to radiation. Other studies using DRS to investigate radiation-induced increase in oxygenation have attributed these changes to increased perfusion [17,28], which typically manifests as an increase in oxygenated hemoglobin (HbO_2). When we investigated the changes in hemoglobin concentration, we found that the increased sO_2 was not due to increased HbO_2 but rather due to a decrease in deoxygenated hemoglobin concentration (dHb). By Day 14, the dHb concentration in the UM-SCC-47 tumors had declined to about 79% of its baseline value while HbO_2 remained unchanged compared

with pre-radiation baseline. A reduction in deoxygenated hemoglobin concentration in the vasculature points to a decrease in oxygen consumption in the surrounding tumor tissue. This would be congruent with a number of studies in the literature, such as one where SCCVII murine tumors treated with 10 Gy of radiation exhibited a reduction in hypoxia found to be caused by a combination of decreased oxygen consumption and increased perfusion [30]. In HNSCC patients treated with daily fractions of 2 Gy (total of 70 Gy), Lyng et al have shown changes in oxygenation, determined by polarographic needles, to coincide with changes in biopsy-determined cell density [31]. Lack of simultaneous changes in vascular density led them to conclude that the observed changes in hypoxia were caused by changes in OCR rather than changes in delivery. Notably, in patients with advanced HNSCC treated with hyperfractionated radiation therapy, Dietz et al found that complete or partial responders show minimal change in reoxygenation in comparison to a strong reoxygenation among nonresponding patients [32].

Although reoxygenation has been considered to lead to cell kill, reoxygenation following radiation can also lead to the generation of reactive oxygen species following hypoxia-reoxygenation injury and hence, the stabilization of HIF-1[33]. This is supported by an elegant study by Moeller et al where mice with 4T1 mammary adenocarcinoma tumors showed HIF-1 activation following radiation that coincided with reoxygenation [27]. We have previously shown that radiation-resistant human lung cancer cells have lower oxygen-consumption rate (OCR) and higher HIF-1 content both at baseline and 24 h after a single dose of 2 Gy compared with their radiation-sensitive counterparts [21]. In addition, we have also shown that increased HIF-1 content leads to increased glucose uptake and hence an increase in reduced glutathione which led to a reduction in mitochondrial reactive oxygen species production. Treatment with a HIF-1 inhibitor led to a decrease in HIF-1, glucose uptake, and reduced glutathione and led to increased cell death in the radiation-resistant cells in comparison with the radiation-sensitive cells [34]. Our observation of a decrease in dHb, a corresponding increase in sO_2, coupled with greater HIF-1α expression both prior to and after radiation therapy in the UM-SCC-47 tumors compared with the UM-SCC-22B tumors strongly suggests that these changes are due to a decrease in oxygen consumption rate and that the reduction in OCR plays a role in radiation resistance. In fact, *in vitro* measurements of oxygen consumption rate revealed lower OCR in UM-SCC-47 cells in comparison to UM-SCC-22B cells (see Supplementary Figure SF5).

However, significant research has demonstrated the clinical value of reducing OCR to improve treatment response by increasing the available oxygen for radiosensitization. Secomb and colleagues showed, using theoretical simulations that utilized experimental observations, that a reduction in oxygen consumption by only 30% was sufficient to completely abolish hypoxia whereas a 4-fold increase in flow rate or a 11-fold increase in arterial pO_2 was required to achieve the same effect [35]. A comprehensive study that measured radiation-induced changes in the tumor microenvironment in the first 24 h proposed that early reoxygenation within tumors was likely due to a combination of increased oxygen supply and a decrease in oxygen consumption [36]. The same group showed that inhibiting mitochondrial respiration using glucocorticoids leads to a reduction in OCR and delayed tumor growth [37]. A more recent study has shown that Arsenic trioxide (As_2O_3) treatment leads to enhanced oxygenation through reduced oxygen consumption in mouse transplantable liver tumors, and its combination with 10 Gy leads to significant delay in tumor growth and extended survival [38]. In addition, Benej et al determined that reducing OCR using Papaverine, a muscle relaxant and mitochondrial complex I inhibitor, significantly decreases hypoxia, improves tumor pO_2, and delays radiation-induced tumor growth [39]. These studies present an interesting juxtaposition – while a reduction in oxygen consumption is clearly beneficial in decreasing hypoxia and hence improving response rates, our work demonstrates that the growing, relatively nonresponsive UM-SCC-47 tumors are likely developing a reduced oxygen consumption rate which is being manifested as a decrease in deoxygenated hemoglobin and hence increased oxygenation. As discussed earlier, our previous work in a matched model of radiation resistance showed that inhibition of HIF-1α led to a reduction in pyruvate dehydrogenase kinase (PDK-1) content [34]. PDK-1 is a negative regulator of pyruvate entry into the mitochondria. Thus, inhibiting PDK-1 increased mitochondrial oxygen consumption and hence cell death in radiation-resistant cells. It will be important to investigate the effects of HIF-1 inhibition *in vivo* to determine if the same phenomenon can be recapitulated in tumors.

HIF-1 also plays an important role in regulating vascular radiosensitivity. Gorski et al showed that radiation caused a large cell line-dependent increase in vascular endothelial growth factor (VEGF) over the first 72 h following treatment and that increased VEGF expression promoted endothelial cell radioresistance [40,41]. Treatment of mice with anti-VEGF prior to radiation therapy led to a significant reduction in tumor growth that was greater than the expected additive effect of the two treatments. Moeller et al found that that VEGF expression overlapped completely with HIF-1 in XT tumors, strongly implicating HIF-1 as a major regulator of endothelial cell radiation resistance due its regulation of VEGF [27]. Although not investigated here, it is possible that the radiation-resistant UM-SCC-47 tumors with their elevated HIF-1 expression also have increased VEGF content, which could have protected the vasculature from radiation-induced damage and hence, promoted radiation resistance.

Although we did not observe any statistically significant differences in tissue scattering between the NT and XT groups of either cell line, we did observed a significant temporal increase in UM-SCC-22B tumors (both NT and XT) over the 14-d period. The increased scattering in the NT group could be attributed to either increased tumor volume, which would increase cell density and hence light scattering from cells, or an increase in tumor hypoxia. We have previously demonstrated a strong association between tumor hypoxic fraction and tissue scattering [16]. However, the temporal changes in scattering in the XT group are intriguing given the lack of change in tumor volume or tumor oxygenation over the 14-d period and seem worthy of further investigation.

Although diffuse reflectance spectroscopic measurements present a promising avenue for studying radiation response in superficial tumors of skin, cervix, and oral cavity, it has limited penetration depth and is not ideal for deep-seated tumors. Sampling depth can be improved by using larger separations between source and detector fibers as well as by extending spectral boundaries to near-infrared (NIR). For example, Sunar et al have demonstrated the utility of NIRS in monitoring chemoradiation induced physiological changes in patients of head and neck cancer [42]. In addition to greater penetration depth, NIR spectroscopy provides more quantitative parameters because of the light absorption by lipid and water at higher wavelengths. A study by Ohmae et al in breast cancer patients, has shown such optical measurements of lipids and water to be highly concordant with computed tomographic measurements [43]. Tromberg et al have used a combination of hemoglobin and lipid absorption as well as scattering to determine a "Tissue optical index" for predicting treatment response in breast cancer patients undergoing neoadjuvant chemotherapy [44]. Multispectral optoacoustic tomography [45–47] and photoacoustic imaging [48,49] is another technique that can provide information about hemoglobin concentration and saturation at depths of up to 7 cm. However, despite its repeated and noninvasive measurements of tissue physiology, multispectral optoacoustic tomography-based systems are currently more expensive than diffuse optical systems.

In summary, we have used diffuse reflectance spectroscopy to monitor tumor hemoglobin oxygen saturation during the course of radiation therapy and found that radiation-resistant HNSCC tumor xenografts show an increase in tumor vascular oxygenation following radiation therapy, a phenomenon not observed in radiation-sensitive HNSCC tumor xenografts. Our analysis of oxygenated and deoxygenated hemoglobin concentrations

following radiation therapy point to decreased oxygen consumption as a likely factor in the increased reoxygenation observed in the UM-SCC-47 tumors. In addition to providing valuable information about functional changes within the tumor at early time points, our study also illustrates the potential of optical spectroscopy of monitoring treatment response in patients and distinguishing between treatment responders and nonresponders. While our work here and elsewhere has explored the important role for HIF-1 in the context of oxygen consumption and metabolism in radiation resistance, HIF-1 also affects other aspects of the tumor microenvironment, such as extracellular matrix remodeling. In addition to monitoring functional changes, we plan to utilize Raman spectroscopy to determine biomolecular changes within the tumor microenvironment during and after radiation therapy. In a recent study, we used Raman spectroscopy on excised tumor xenografts to demonstrate differences in biomolecular composition, specifically lipids and collagen, in XT and nNT UM-SCC-22B and UM-SCC-47 tumors [50]. Based on these differences, we were able to accurately distinguish radiation-sensitive from responsive tumors. A combination of diffuse reflectance and Raman spectroscopy to simultaneously monitor radiation-induced functional and biomolecular changes within the tumor *in vivo* could improve our understanding of microenvironmental changes related to treatment resistance. Subsequently, we could identify patients with likely nonresponsive tumors earlier in the treatment regimen, allowing critical adjustments to be made to the treatment plan.

Supplementary materials

Supplementary material associated with this article can be found, in the online version, at doi:10.1016/j.neo.2020.11.006.

CRediT authorship contribution statement

Sina Dadgar: Conceptualization, Methodology, Investigation, Formal analysis, Project administration, Visualization, Writing - original draft, Writing - review & editing. **Joel Rodriguez Troncoso:** Methodology, Investigation. **Eric R. Siegel:** Formal analysis, Writing - original draft, Writing - review & editing, Funding acquisition. **Natalie M. Curry:** Methodology, Investigation. **Robert J. Griffin:** Conceptualization, Writing - review & editing, Funding acquisition. **Ruud P.M. Dings:** Conceptualization, Writing - review & editing, Funding acquisition. **Narasimhan Rajaram:** Conceptualization, Methodology, Investigation, Resources, Writing - review & editing, Supervision, Funding acquisition.

References

[1] Worsham MJ. Identifying the risk factors for late-stage head and neck cancer. *Expert Rev Anticancer Ther* 2011. doi:10.1586/era.11.135.

[2] Marur S, Forastiere AA. Head and neck squamous cell carcinoma: update on epidemiology, diagnosis, and treatment. *Mayo Clin Proc* 2016. doi:10.1016/j.mayocp.2015.12.017.

[3] Fowler J. The rational of dose fractionation. *The Relationship of Time and Dose in the Radiation Therapy of Cancer.*. Karger Publishers; 1969. in 6–23.

[4] Kallman RF. The phenomenon of reoxygenation and its implications for fractionated radiotherapy. *Radiology* 1972;**105**:135–42.

[5] Withers HR. The 4 Rs of radiotherapy. *Adv. Radiat. Biol.* 1975;**5**:241–71.

[6] Brizel DM, Sibley GS, Prosnitz LR, Scher RL, Dewhirst MW. Tumor hypoxia adversely affects the prognosis of carcinoma of the head and neck. *Int. J. Radiat Oncol Bio. Phys.* 1997. doi:10.1016/S0360-3016(97)00101-6.

[7] Nordsmark M, Bentzen S, Rudat V, Brizel D, Lartigau E, Stadler P, Becker A, Adam M, Molls M, Dunst J, et al. Prognostic value of tumor oxygenation in 397 head and neck tumors after primary radiation therapy. An international multi-center study. *Radiother Oncol.* 2005. doi:10.1016/j.radonc.2005.06.038.

[8] Brizel DM, Dodge RK, Clough RW, Dewhirst MW. Oxygenation of head and neck cancer: changes during radiotherapy and impact on treatment outcome. *Radiothe. Oncol.* 1999;**53**:113–17.

[9] Rudat V, Stadler P, Becker A, Vanselow B, Dietz A, Wannenmacher M, Molls M, Dunst J, Feldman HJ. Predictive value of the tumor oxygenation by means of pO2histography in patients with advanced head and neck cancer. *Strahlenther Onkol* 2001. doi:10.1007/PL00002427.

[10] Milas L, Hunter NR, Mason KA, Milross CG, Saito Y, Peters LJ. Role of reoxygenation in induction of enhancement of tumor radioresponse by paclitaxel. *Cancer Res* 1995.

[11] Ressel A, Weiss C, Feyerabend T. Tumor oxygenation after radiotherapy, chemotherapy, and/or hyperthermia predicts tumor free survival. *Int. J. Radiat. Oncol. Biol. Phys.* 2001;**49**:1119–25.

[12] Rajaram N, Nguyen TH, Tunnell JW. Lookup table–based inverse model for determining optical properties of turbid media. *J Biomed Opt.* 2008;**13**:050501.

[13] Nichols BS. Performance of a lookup table-based approach for measuring tissue optical properties with diffuse optical spectroscopy. *J Biomed Opt.* 2012;**17**:057001.

[14] Palmer GM, Viola RJ, Schroeder T, Yarmolenko PS, Dewhirst MW, Ramanujam N. Quantitative diffuse reflectance and fluorescence spectroscopy: tool to monitor tumor physiology *in vivo*. *J Biomed Opt.* 2012;**14**:024010.

[15] Wang HW, Putt ME, Emanuele MJ, Shin DB, Glatstein E, Yodh AG, Busch TM. Treatment-induced changes in tumor oxygenation predict photodynamic therapy outcome. *Cancer Res* 2004;**64**:7553–61.

[16] Dadgar S, Troncoso JR, Rajaram N. Optical spectroscopic sensing of tumor hypoxia. *J Biomed Opt.* 2018;**23**:1–10.

[17] Hu F, Vishwanath K, Salama JK, Erkanli A, Peterson B, Oleson JR, Lee WT, Brizel DM, Ramanujam N, Dewhirst MW. Oxygen and perfusion kinetics in response to fractionated radiation therapy in FaDu head and neck cancer xenografts are related to treatment outcome. *Int J Radiat Oncol Biol Phys.* 2016;**96**:462–9.

[18] Diaz PM, Jenkins SV, Alhallak K, Semeniak D, Griffin RJ, Dings RPM, Rajaram N. Quantitative diffuse reflectance spectroscopy of short-term changes in tumor oxygenation after radiation in a matched model of radiation resistance. *Biomed Opt Express* 2018;**9**:3794.

[19] Kimple RJ, Smith MA, Blitzer GC, Torres AD, Martin JA, Yang RZ, Peet CR, Lorenz LD, Nickel KP, Klingelhutz AJ, et al. Enhanced radiation sensitivity in HPV-positive head and neck cancer. *Cancer Res* 2013. doi:10.1158/0008-5472.CAN-13-0587.

[20] Stein AP, Swick AD, Smith MA, Blitzer GC, Yang RZ, Saha S, Harrari PM, Lambert PF, Liu CZ, Kimple RJ. Xenograft assessment of predictive biomarkers for standard head and neck cancer therapies. *Cancer Med* 2015;**4**:699–712.

[21] Alhallak K, Jenkins SV, Lee DE, Greene NP, Quinn KP, Griffin RJ, Dings RPM, Rajaram N. Optical imaging of radiation-induced metabolic changes in radiation- sensitive and resistant cancer cells. *J Biomed Opt.* 2017;**22**:60502.

[22] Greening GJ, Miller KP, Spainhour CR, Cato MD, Muldoon TJ. Effects of isoflurane anesthesia on physiological parameters in murine subcutaneous tumor allografts measured via diffuse reflectance spectroscopy. *Biomed Opt Express* 2018. doi:10.1364/boe.9.002871.

[23] Mourant JR, Fuselier T, Boyer J, Johnson TM, Bigio IJ. Predictions and measurements of scattering and absorption over broad wavelength ranges in tissue phantoms. *Appl. Opt.* 1997. doi:10.1364/AO.36.000949.

[24] Prahl S. Optical absorption of hemoglobin. *Portland: Oregon MedLaser Center* 2015.

[25] Rajaram N, Gopal A, Zhang X, Tunnell JW. Experimental validation of the effects of microvasculature pigment packaging on *in vivo* diffuse reflectance spectroscopy. *Lasers Surg. Med.* 2010;**42**:680–8.

[26] Dings RPM, Loren M, Heun H, McNiel E, Griffioen AJ, Mayo KH, Griffin RJ. Scheduling of radiation with angiogenesis inhibitors anginex and avastin improves therapeutic outcome via vessel normalization. *Clin Cancer Res.* 2007. doi:10.1158/1078-0432.CCR-06-2441.

[27] Moeller BJ, Cao Y, Li CY, Dewhirst MW. Radiation activates HIF-1 to regulate vascular radiosensitivity in tumors: role of reoxygenation, free radicals, and stress granules. *Cancer Cell* 2004;**5**:429–41.

[28] Vishwanath K, Klein D, Chang K, Schroeder T, Dewhirst MW, Ramanjuam N. Quantitative optical spectroscopy can identify long-term local tumor control in irradiated murine head and neck xenografts. *J. Biomed. Opt.* 2009;**14**:054051.

[29] Stadler P, Feldmann HJ, Creighton C, Kau R, Molls M. Changes in tumor oxygenation during combined treatment with split- course radiotherapy and chemotherapy in patients with head and neck cancer. *Radiother Oncol.* 1998. doi:10.1016/S0167-8140(98)00032-2.

[30] Olive PL. Radiation-induced reoxygenation in the SCCVII murine tumour: evidence for a decrease in oxygen consumption and an increase in tumour perfusion. *Radiother Oncol.* 1994. doi:10.1016/0167-8140(94)90447-2.

[31] Lyng H, Tanum G, Evensen JF, Rofstad EK. Changes in oxygen tension during radiotherapy of head and neck tumours. *Acta Onco. (Madr).* 1999. doi:10.1080/028418699432329.

[32] Dietz A, Vanselow B, Rudat V, Conradt C, Weidauer Hagen, Kallinowski F, Dollner R. Prognostic impact of reoxygenation in advanced cancer of the head and neck during the initial course of chemoradiation or radiotherapy alone. *Head Neck* 2003;**25**:50–8.

[33] Chandel NS, McClintock DS, Feliciano CE, Wood TM, Melendez JA, Rodriguez AM, Schumcker PT. Reactive oxygen species generated at mitochondrial Complex III stabilize hypoxia-inducible factor-1α during hypoxia: A mechanism of O2 sensing. *J. Biol. Chem.* 2000;**279**:25130–8.

[34] Lee DE, Alhallak K, Jenkins SV, Vargas I, Greene NP, Quinn KP, Griffin RJ, Dings RPM, Rajaram N. A Radiosensitizing Inhibitor of HIF-1 alters the Optical Redox State of Human Lung Cancer Cells in Vitro. *Sci. Rep.* 2018;**8**:8815.

[35] Secomb TW, Hsu R, Ong ET, Gross JF, Dewhirst MW. Analysis of the effects of oxygen supply and demand on hypoxic fraction in tumors. *Acta Oncol. (Madr)* 1995. doi:10.3109/02841869509093981.

[36] Crokart N, Jordan BF, Baudelet C, Ansiaux R, Sonveaux P, Gregoire V, Beghein N, DeWever J, Bouzin C, Feron O, et al. Early reoxygenation in tumors after irradiation: Determining factors and consequences for radiotherapy regimens using daily multiple fractions. *Int. J. Radiat. Oncol. Biol. Phys.* 2005. doi:10.1016/j.ijrobp.2005.02.038.

[37] Crokart N, Jordan BF, Baudelet C, Cron GO, Hotton J, Radermacher K, Gregoire V, Beghein N, Martinive P, Bouzin C, et al. Glucocorticoids modulate tumor radiation response through a decrease in tumor oxygen consumption. *Clin. Cancer Res.* 2007. doi:10.1158/1078-0432.CCR-06-0802.

[38] Diepart C, Karroum O, Magat J, Feron O, Verrax J, Calderon PB, Gregoire V, Leveque P, Stockis J, Dauguet N, et al. Arsenic trioxide treatment decreases the oxygen consumption rate of tumor cells and radiosensitizes solid tumors. *Cancer Res.* 2012. doi:10.1158/0008-5472.CAN-11-1755.

[39] Benej M, Hong X, Vibhute S, Scott S, Wu J, Graves E, Le QT, Koong AC, Giaccia AJ, Yu B, et al. Papaverine and its derivatives radiosensitize solid tumors by inhibiting mitochondrial metabolism. *Proc. Natl. Acad. Sci. U. S. A.* 2018. doi:10.1073/pnas.1808945115.

[40] Gorski DH, Beckett MA, Jaskowiak NT, Calvin DP, Mauceri HJ, Salloum RM, Seetharam S, Koons A, Hari DM, Kufe DW, et al. Blockade of the vascular endothelial growth factor stress response increases the antitumor effects of ionizing radiation. *Cancer Res.* 1999.

[41] Gupta VK, Jaskowiak NT, Beckett MA, Mauceri HJ, Grunstein J, Johnson RS, Calvin DA, Nodzenski E, Pejovic M, Kufe DW, et al. Vascular endothelial growth factor enhances endothelial cell survival and tumor radioresistance. *Cancer J.* 2002. doi:10.1097/00130404-200201000-00009.

[42] Sunar U, Quon H, Durduran T, Zhang J, Du J, Zhou C, Yu G, Choe R, Kilger A, Lustig RA, et al. Noninvasive diffuse optical measurement of blood flow and blood oxygenation for monitoring radiation therapy in patients with head and neck tumors: a pilot study. *J. Biomed. Opt.* 2007. doi:10.1117/1.2397548.

[43] Ohmae E, Yoshizawa N, Yoshimoto K, Hayashi M, Wada H, Mimura T, Asano Y, Ogura H, Yamashita Y, Sakahara H, et al. Comparison of lipid and water contents by time-domain diffuse optical spectroscopy and dual-energy computed tomography in breast cancer patients. *Appl. Sci.* 2019. doi:10.3390/app9071482.

[44] Tromberg BJ, Zhang Z, Leproux A, O'Sullivan TD, Cerussi AE, Carpenter PM, Mehta RS, Roblyer D, Yang W, Paulsen KD, et al. Predicting responses to neoadjuvant chemotherapy in breast cancer: ACRIN 6691 trial of diffuse optical spectroscopic imaging. *Cancer Res.* 2016;**76**:5933–44.

[45] Tomaszewski MR, Gonzalez IQ, O'Connor JP, Abeyakoon O, Parker GJ, Williams KJ, Gilbert FJ, Bohndiek SE. Oxygen enhanced Optoacoustic Tomography (OE-OT) reveals vascular dynamics in murine models of prostate cancer. *Theranostics* 2017;**7**:2900–13.

[46] Tomaszewski MR, Gehrung M, Joseph J, Gonzalez IQ, Disselhorst JA, Bohndiek SE. Oxygen-enhanced and dynamic contrast- enhanced optoacoustic tomography provide surrogate biomarkers of tumor vascular function, hypoxia, and necrosis. *Cancer Res.* 2018. doi:10.1158/0008-5472.CAN-18-1033.

[47] Ghosh P, Guo Y, Ashrafi A, Chen J, Dey S, Zhong S, Liu J, Campbell J, Konduri PC, Gerberich J, et al. Oxygen-Enhanced Optoacoustic Tomography Reveals the Effectiveness of Targeting Heme and Oxidative Phosphorylation at Normalizing Tumor Vascular Oxygenation. *Cancer Res.* 2020. doi:10.1158/0008-5472.can-19-3247.

[48] Zackrisson S, Van De Ven SMWY, Gambhir SS. Light in and sound out: Emerging translational strategies for photoacoustic imaging. *Cancer Res.* 2014. doi:10.1158/0008-5472.CAN-13-2387.

[49] Rich LJ, Seshadri M. Photoacoustic monitoring of tumor and normal tissue response to radiation. *Sci. Rep.* 2016. doi:10.1038/srep21237.

[50] Paidi SK, Diaz PM, Dadgar S, Jenkins SV, Quick CM, Griffin RJ, Dings RPM, Rajaram N, Barman B. Label-free Raman spectroscopy reveals signatures of radiation resistance in the tumor microenvironment. *Cancer Res* 2019;**79**:2054–64.